Geosci. Model Dev. Discuss., doi:10.5194/gmd-2016-163, 2016
Manuscript under review for journal Geosci. Model Dev.
Published: 11 August 2016
© Author(s) 2016. CC-BY 3.0 License.

Geoscientific Model Development Discussions
Open Access
EGU

Constraining a hybrid volatility basis set model for aging of wood burning emissions using smog chamber experiments

Giancarlo Ciarelli[1], Imad El Haddad[1], Emily Bruns[1], Sebnem Aksoyoglu[1], Ottmar Möhler[2], Urs Baltensperger[1] and André S.H. Prévôt[1].

[1]{Paul Scherrer Institute, Laboratory of Atmospheric Chemistry, 5232 Villigen PSI, Switzerland}
[2]{Karlsruhe Institute of Technology, Institute of Meteorology and Climate Research, Germany}

Correspondence to: I. El Haddad and S. Aksoyoglu (imad.el-haddad@psi.ch and sebnem.aksoyoglu@psi.ch)

Abstract

Semi-volatile and intermediate volatility organic compounds (SVOCs, IVOCs) are not included in the current non-methane volatile organic compounds (NMVOCs) emission inventories but may be important for the formation of secondary organic aerosol (SOA). In this study, novel wood combustion aging experiments performed at different temperatures (263 K and 288 K) in a ~7 m^3 smog chamber were modelled using a hybrid volatility basis set (VBS) box model, representing the emission partitioning and their oxidation against OH. We combine aerosol-chemistry box model simulations with unprecedented measurements of non-traditional volatile organic compounds (NTVOCs) from a high-resolution proton transfer reaction mass spectrometer (PTR-MS) and with organic aerosol measurements from an aerosol mass spectrometer (AMS). In so-doing, we are able to observationally-constrain the amounts of different NTVOCs aerosol precursors (in the model) relative to low-volatility and semi-volatile primary organic material (OM_{sv}) which is partitioned based on current published volatility distribution data. By comparing the NTVOCs/OM_{sv} ratios at different temperatures, we determine the enthalpies of vaporization of primary biomass burning organic aerosols. Further, the developed model allows for evaluating the evolution of oxidation products of the semi-volatile and volatile precursors with aging. More than 30,000 box model simulations were performed to retrieve the combination of parameters that fit best the observed organic aerosol mass and O:C ratios. The parameters investigated include the NTVOC reaction rates and yields as well as enthalpies of vaporization and the O:C of secondary organic aerosol surrogates. Our results suggest an average ratio of NTVOCs to the sum of non-volatile and

Geosci. Model Dev. Discuss., doi:10.5194/gmd-2016-163, 2016
Manuscript under review for journal Geosci. Model Dev.
Published: 11 August 2016
© Author(s) 2016. CC-BY 3.0 License.

Geoscientific Model Development Discussions

semi-volatile organic compounds of ~4.75. The mass yields of these compounds determined for a wide range of atmospherically relevant temperatures and organic aerosol (OA) concentrations were predicted to vary between 8 and 30 % after 5 hours of continuous aging. Based on the reaction scheme used, reaction rates of the NTVOC mixture range from 3.0 x 10^{-11} cm^3 $molec^{-1}$ s^{-1} to 4.0 x 10^{-11} cm^3 $molec^{-1}$ s^{-1}. The average enthalpy of vaporization of SOA surrogates was determined to be between 55,000 J mol^{-1} and 35,000 J mol^{-1} which implies a yield increase of 0.03 - 0.06 % K^{-1} with decreasing temperature. The improved VBS scheme is suitable for implementation into chemical transport models to predict the burden and oxidation state of primary and secondary biomass burning aerosols.

1 Introduction

The fact that some semi-volatile compounds can exist in either gaseous or particulate form results in considerable uncertainties in the emission inventories for fine particulate matter ($PM_{2.5}$) and non-methane volatile organic compounds (NMVOCs). Emissions of $PM_{2.5}$ are generally based on emission factors (EF) of primary organic aerosol (POA) which may be over- or under-predicted depending on the measurement method used (Lipsky and Robinson, 2006; Nussbaumer et al., 2008a, 2008b.).

In Europe, residential wood-burning emissions constitute one of the main anthropogenic sources of POA and potentially secondary organic aerosol (SOA), especially during winter periods with contribution from 15% to 50% of the total organic mass (Crippa et al., 2013; Waked et al., 2014). Thus, great effort was devoted in the past to better constrain the uncertainties related to wood burning emissions and their evolution in the atmosphere (Denier van der Gon et al., 2015; May et al., 2013). Recent year-long source apportionment studies based on ACSM (aerosol chemical speciation monitor) measurements in central Europe suggest that winter secondary organic aerosol fingerprints resembles those measured during chamber studies of biomass burning emission aging (Canonaco et al., 2015).

One of the main complications when dealing with organic aerosol (OA) is imposed by the semi-volatile and highly reactive nature of organic material (Robinson et al., 2007). Depending on ambient conditions freshly emitted primary organic particles can undergo evaporation. The fraction of an organic compound *i* in the condensed phase can be inferred based on the absorptive partitioning theory of Pankow (1994) (Eq. 1). The critical parameters driving the gas-particle partitioning of this compound are its effective saturation concentration, C_i^*, and the total concentration of organic aerosol, C_{OA}:

Geosci. Model Dev. Discuss., doi:10.5194/gmd-2016-163, 2016
Manuscript under review for journal Geosci. Model Dev.
Published: 11 August 2016
© Author(s) 2016. CC-BY 3.0 License.

Geoscientific Model Development Discussions

$$\xi_i = \left(1 + \frac{C_i^*}{C_{OA}}\right)^{-1}; C_{OA} = \sum_i \xi_i C_i, \quad (1)$$

Here, ξ_i is the partitioning coefficient of i (condensed-phase mass fraction). C_i^* is a semi-empirical property (inverse of the Pankow-type partitioning coefficient, K_P), reflecting not only the saturation vapor pressure of the pure constituents $\left(p_{L,i}^o\right)$ but also the way they interact with the organic mixture (effectively including liquid phase activities). This formulation essentially determines that at high C_{OA} almost all semi-volatile organic aerosols are in the condensed phase with only species with the highest vapour pressures remaining in the gas phase.

The volatility basis set approach (VBS) was proposed by Donahue et al., (2006) to provide a framework to enable models to represent both the chemical ageing and the associated evolving volatility of particulate organic matter in the atmosphere. The approach is to separate organics into logarithmically spaced bins of effective saturation concentrations C_i^*, at 298 K and it was later extended (Donahue et al., 2011, 2012) by introducing surrogate compounds with different carbon and oxygen numbers following the group contribution approach based on the SIMPOL method (Pankow and Asher, 2008) (Equation 2). The model becomes 2-dimensional, capable of tracking compound volatility and oxidation state (O:C ratios) (Donahue et al., 2011, 2012):

$$\log_{10} C_i^0 = \left(n_C^0 - n_C^i\right) b_C - n_O^i b_O - 2\frac{n_C^i n_O^i}{n_C^i + n_O^i} b_{CO} \quad (2)$$

where b_c and b_O represent the carbon-carbon and oxygen-oxygen interactions, respectively, b_{CO} describes the non-ideal solution behaviour and n_C^0 , equal to 25, represents the reference point for pure hydrocarbons (1 μg m^{-3} of alkene). n_C^i and n_O^i are the carbon and oxygen numbers, respectively, for the ith saturation concentration (C_i^0). For biomass burning in particular, May et al. (2013) revealed that the majority of the emitted primary OA mass is semi-volatile, with 50 to 80 % of the POA mass evaporating when diluted from plume to ambient concentrations or when heated up to 100°C in a thermodenuder. Based on their results, they proposed a volatility distribution function and enthalpies of vaporization for wood burning smoke (May et al., 2013).

Once emitted in the atmosphere, organic compounds are highly reactive towards various oxidants such as the hydroxyl radical (OH), ozone (O_3) and the nitrate radical (NO_3). These oxidants can strongly alter the chemical structure of the reacted precursors by generating

Geosci. Model Dev. Discuss., doi:10.5194/gmd-2016-163, 2016
Manuscript under review for journal Geosci. Model Dev.
Published: 11 August 2016
© Author(s) 2016. CC-BY 3.0 License.

secondary products with lower or higher volatilities. Linking partitioning and oxidation processes of thousands of emitted organic compounds is one of the main challenges in atmospheric chemistry. The VBS scheme can delineate the transformation of the surrogates upon their functionalization or fragmentation, by changing the compounds' volatility and O:C ratios, consistently with the dominant representative species in that part of the parameter space. Chemical transport models (CTMs) have been increasingly updated with a VBS scheme with varying complexities (Bergström et al., 2012; Ciarelli et al., 2016; Murphy et al., 2011; Zhang et al., 2013). A recent landmark paper within the international AeroCom initiative (Tsigaridis et al., 2014), gave a comprehensive audit of the status of organic aerosol schemes in global models, brought together several benchmark observational datasets and intercompared and evaluated the OA simulated by a large number of global aerosol models against them. Results indicate that simulated OA greatly varies between models in terms of POA emissions, SOA formation and complexity of OA parameterizations and the amount of OA remains under-predicted. In the latest EURODELTA3 (EUIII) European model intercomparison, seven different regional models were applied in the European domain during different periods with a focus on the February-March 2009 EUCAARI winter episode (Bessagnet et al., 2014). All models under-predicted the total measured organic fraction mainly due the uncertainties in SOA representation (Bessagnet et al., 2014). Knote et al. (2011) used the COSMO-ART model to investigate its performance as online-coupled chemistry-climate model. In their study domestic wood burning emissions were not included and POA was assumed to be non-volatile, which resulted in a severe under-prediction of OA over the studied domain (Knote et al., 2011). Bergström et al. (2012) used the EMEP model for the period of 2002-2007 comparing different partitioning and aging schemes, and their results indicate a potential underestimation of wood-burning emissions in Europe. Founoukis et al. (2014) were among the first to implement the VBS approach into a large-scale aerosol model, following the multiple distribution framework approach proposed by Tsimpidi et al. (2010). They found the approach improved considerably the OA simulated in the model across Europe comparing to a range of observations made during the EUCAARI field campaign (Kulmala et al., 2009, 2011) and from EMEP monitoring network (Tørseth et al., 2012). Recently, an important new initiative to provide improved information on residential wood combustion (RWC) emission inventory for Europe was carried out by Denier van der Gon et al. (2015) and used as an input in two CTMs (PMCAMx and EMEP MSC-W) for the EUCAARI winter periods (February-March 2009). The new RWC emissions, which are

Geosci. Model Dev. Discuss., doi:10.5194/gmd-2016-163, 2016
Manuscript under review for journal Geosci. Model Dev.
Published: 11 August 2016
© Author(s) 2016. CC-BY 3.0 License.

higher by a factor of 2-3 compared to previous emission inventories, improved the model performance for total OA (Denier van der Gon et al., 2015). Jo et al. (2013) deployed the GEOS-Chem global model to investigate the effect of using different aging constants on modelled SOA. They concluded that model simulations are improved when chemical aging is taken into account, especially for rural regions (Jo et al., 2013). These novel investigations highlight the critical need for a representation of semi-volatile organic species and their evolution in chemical transport models.

In this study we perform extensive box-model simulations of wood burning combustion aging experiments performed in a ~7 m^3 smog chamber at different temperatures. Most uncertain parameters namely enthalpies of vaporization of SOA, NTVOCs reaction rates and their yields were investigated by means of brute force simulations, and a best fitting solution, within acceptable physical and errors ranges, was retrieved.

2 Experimental Method

Beech (*Fagus sylvatica*) logs were combusted in a residential wood burner (model type: Avant, Attika from 2009), following the procedure described in (Heringa et al., 2012) and (Bruns et al., 2015). The resulting emissions were sampled from the chimney through a heated line (473 K), diluted by a factor of ~8-10 using an ejector diluter (473 K, DI-1000, Dekati Ltd.) and injected into the smog chamber (~7 m^3) through a heated line (423 K). Emissions were only sampled during the stable flaming phase of the burn, for 11-21 min and total dilution factors ranged from ~100 to 200. Four replicate experiments were conducted at 288 K and another four experiments at 263 K. The smog chamber had an average relative humidity of 50% over all eight experiments. Another three experiments were conducted at 90% relative humidity and 263 K. After the characterization of the primary emissions, a single dose of d9-butanol (butanol-D9, 98%, Cambridge Isotope Laboratories) was injected into the chamber, to trace the OH concentration (Barmet et al., 2012). A continuous flow of nitrous acid (2.3-2.6 l min^{-1}, ≥99.999%, Air Liquide) into the chamber served as an OH precursor. The chamber was then irradiated with UV light (40 lights, 90-100 W, Cleo Performance, Philips) for 4.5-6 h (Platt et al., 2013). The evolution of the gas-phase and particulate phase composition and concentration were monitored in real-time throughout aging. Non-refractory primary and secondary particulate emissions were characterized using a high resolution time-of-flight aerosol mass spectrometer (AMS). Equivalent black carbon

Geosci. Model Dev. Discuss., doi:10.5194/gmd-2016-163, 2016
Manuscript under review for journal Geosci. Model Dev.
Published: 11 August 2016
© Author(s) 2016. CC-BY 3.0 License.

(eBC) was quantified using a 7-wavelength aethalometer (AE33 Magee Scientific Company, flow rate 2 l min^{-1}) (Drinovec et al., 2015). Particle wall loss rates in the chamber were determined using the decay of eBC assuming all particles were lost equally to the walls and that condensable material partitions only to suspended particles. The average particle half-life in the chamber was 3.4±0.7 h. Non-methane organic gases with a proton affinity greater than that of water were measured using a a high-resolution proton transfer reaction mass spectrometer (PTR-ToF-MS 8000, Ionicon Analytik G.m.b.H.). The PTR-ToF-MS was operated with hydronium ($[H_2O+H]^+$) as reagent, a drift tube pressure of 2.2 mbar, a drift tube voltage of 543 V and a drift tube temperature of 90°C leading to a ratio of the electric field (E) and the density of the buffer gas (N) in the drift tube (E/N) of 137 Townsend (Td). The analysis of data PTR-ToF-MS data and the identification of the precursors' chemical nature are described in Bruns et al. (2016). The elemental composition of the detected gases was analyzed using the Tofware post-processing software (version 2.4.5), running in the Igor Pro 6.3 environment (version 6.3, Wavemetrics Inc.). More than 95% of the detected peaks could be assigned to a molecular formula. Approximately 70% of the compounds' chemical structures could be assigned to the observed ions guided by previously reported compounds emitted during residential wood combustion. Here, the lumped sum of the precursors' molar concentrations will be used to constrain the total amount of NTVOCs (Table S1) in the model. Their weighted average O:C ratio, volatility, reaction rate and carbon number will also be presented.

3 Box model

The modelling approach involves two steps.

(1) We first modelled the partitioning of POA for the 11 smog chamber experiments (8 experiments at RH=50% and 3 experiments at RH=90%) before the start of the aging. This step enables constraining the amounts of material in the different volatility bins and the enthalpy of vaporization of the different surrogates used. The simulations proceeded as follows. Using already available volatility distribution data for primary wood burning emissions (Figure 1) we inferred the total amount of organic material (gas and particle phase) in the low-volatility and semi-volatile ranges (OM_{sv}), ($0.1 < C_i^* < 1000$ µg m^{-3}), which matched the measured OA concentrations at the beginning of the experiments ($OA_{t=0}$). The amount of OM_{sv} was then compared to the measured

Geosci. Model Dev. Discuss., doi:10.5194/gmd-2016-163, 2016
Manuscript under review for journal Geosci. Model Dev.
Published: 11 August 2016
© Author(s) 2016. CC-BY 3.0 License.

NTVOCs, at high and low temperatures and the enthalpies of vaporization of primary compounds were adjusted such that a comparable NTVOCs/OM_{sv} ratio was obtained at both temperatures within our experimental variability. We tested several sets of enthalpies of vaporization characteristic of biomass burning OA derived from May et al. (2013); the different sets were all physically possible and were determined from thermodesorber data by assuming different accommodation coefficients.

(2) In step 2, the obtained volatility distributions were used to model the aging of the emissions and SOA formation within a hybrid VBS framework. This framework is adapted from Koo et al. (2014); it describes the formation and further evolution of SOA species from different families of precursors. Unlike previous 2D-VBS schemes, the molecular space was not discretised according to the species saturation concentration and oxidation state (e.g. O:C ratios), but rather every SOA surrogate was given an average molecular composition – $C_xH_yO_z$) – as a function of its volatility and the precursor it derived from. This approach significantly decreases the degree of freedom of the model, while still providing a means to evaluate the bulk aerosol oxidation state based on the knowledge of the surrogate molecular composition. The time-dependent OA mass and O:C ratios were used as model constraints. For step 2, only experiments performed at RH=50% were used, as high RH might favour further uptake of secondary organic material into the bulk phase, effectively increasing aerosol yields (Zuend and Seinfeld, 2012). Such effects are beyond the scope of this study.

In the present study, the bulk micro-physical properties of the condensed phased were not measured. Therefore, for all calculations, we assumed instantaneous reversible absorptive equilibrium of semi-volatile organic species into a well-mixed liquid phase. I.e. the model does invoke diffusion limitations within the condensed phase. These assumptions may influence our results, especially at lower temperatures (e.g. if diffusion limitations were to be considered, higher reaction rates would be required to explain the observations). However, the same assumptions are considered in CTMs and therefore we expect that resulting biases will partially cancel out, providing that the bulk phase properties of chamber and ambient aerosols are not significantly different.

Five volatility bins ranging from 0.1 to 1000 μg m^{-3} in saturation concentration were used to model the partitioning of the POA and SOA fractions. The weighted average carbon and

Geosci. Model Dev. Discuss., doi:10.5194/gmd-2016-163, 2016
Manuscript under review for journal Geosci. Model Dev.
Published: 11 August 2016
© Author(s) 2016. CC-BY 3.0 License.

oxygen numbers of the NTVOCs mixture retrieved from PTR-MS measurements were used in combination with the group contribution approach (Eq. 2) to estimate the average saturation concentration for SOA precursors yielding about ~10^6 μg m^{-3}, which falls within the IVOC saturation concentration range limit (Donahue et al., 2012; Koo et al., 2014; Murphy and Pandis, 2009) (Figure 2).

A total number of 3 sets were chosen to describe the evolution of organic material. The first set was used to distribute the primary emissions (set1). Two other sets were used to model the formation and evolution of SOA. Oxidation products of SVOC material arising from primary emissions were allocated to set2, whereas oxidation products from NTVOCs were allocated to set3 (Figure 3).

The specific molecular structures for each of the sets and bins were retrieved using the group contribution approach and the Van Krevelen relation (Table 1). Primary wood burning emissions were placed to range from 14 to 11 carbons (set1) in line with previous studies (Donahue et al., 2012; Koo et al., 2014) and appropriate numbers of oxygen atoms were retrieved (Eq. 2). The oxidation of semi-volatile material would tend to increase the compounds' oxygen number and decrease their volatility and carbon number, due to functionalization and fragmentation. We assume that the oxidation of the primary semi-volatile compounds with C_{11}-C_{14} decreases their volatility by one order of magnitude and yields C_9-C_{10} surrogates, placed in set2, based on the work of Donahue et al. (2011, 2012). Based on these assumptions and using the group contribution approach, the oxygen numbers for set 2 is predicted to vary between 2.26 and 4.56 (Figure 2). Thus, the model implicitly accounts for the addition of 1.1 to 1.5 oxygen atoms and the loss of 2.75 to 4.25 carbon atoms, with one oxidation step.

Set3, was directly constrained based on the PTR-MS data. The measurements suggested an average NTVOC carbon and oxygen number of about 7 and 1, respectively. Based on reported molecular speciation data (Kleindienst et al., 2007), we expect that the products of C_7 compounds have a C_5-C_6 carbon backbone. These products were placed in set3 following a kernel function based on the distribution of naphthalene oxidation products. At least two oxygens atoms were added to the NTVOC mixture upon their oxidation (Figure 2 and Figure 3). The overall, O:C ratio in the whole space roughly spans the range from 0.1 to 1.0.

Multigeneration chemistry (aging) is also accounted for by the model. Gas-phase products in the semi-volatile range in set2 and set3, once formed, can further react with a rate constant of

Geosci. Model Dev. Discuss., doi:10.5194/gmd-2016-163, 2016
Manuscript under review for journal Geosci. Model Dev.
Published: 11 August 2016
© Author(s) 2016. CC-BY 3.0 License.

Geoscientific Model Development Discussions

4 x 10^{-11} cm^3 $molecule^{-1}$ s^{-1} as proposed by previous studies (Donahue et al., 2013; Grieshop et al., 2009; Robinson et al., 2007), further lowering the volatility of the products by one order of magnitude.

As the modelled species' average carbon number systematically decreases with aging, this approach effectively takes into consideration the compounds' fragmentation. In parallel, the addition of oxygen reflects the compounds' functionalization with aging and the increase in the measured O:C ratio. Therefore, unlike previous 2D-VBS schemes where functionalization and fragmentation are disentangled, the approach adopted here, by decreasing the number of carbon atoms and increasing the number of oxygens atoms, simultaneously describes both processes.

In addition to the constrains mentioned above, three parameters were determined based on experimentally constrained time-dependent OA mass and O:C ratios, i.e., NTVOCs reaction rates and yields as well as average enthalpies of vaporization values for the set 2 and 3. Detailed explanations are presented in the next two sections.

3.1.1 Inferring OM_{sv} and NTVOCs/OM_{sv} ratios from measurements and partitioning theory

We seek to determine, based on the PTR-MS and AMS measurements of gas and particle phase organic material at t=0, the ratio NTVOCs/OM_{sv} and the enthalpies of vaporization of compounds of the semi-volatile compounds that represent best the observations at high and low temperatures. We modelled the $OA_{t=0}$ partitioning using two different proposed ΔH_{vapPOA} for wood burning:

$$\Delta H_{vapPOA} = -4 \log_{10}(C^*_{298K}) + 85 \quad (3)$$

$$\Delta H_{vapPOA} = -11 \log_{10}(C^*_{298K}) + 70 \quad (4)$$

Eq. 3 is the best fitting solution proposed by May et al. (2013), while Eq. 4 represents the lower limit for ΔH_{vapPOA} for a solution within the range of experimental uncertainties (Figure 4 in May et al. 2013). We will refer to these solutions as SOL1 for Eq. 3, and SOL2 for Eq. 4. Table 2 reports the measured $OA_{t=0}$ for all the 11 experiments, which ranges from 6.0 µg m^{-3}

Geosci. Model Dev. Discuss., doi:10.5194/gmd-2016-163, 2016
Manuscript under review for journal Geosci. Model Dev.
Published: 11 August 2016
© Author(s) 2016. CC-BY 3.0 License.

and 22.6 μg m^{-3}. The amount of OM_{sv} that matches the measured $OA_{t=0}$ is reported for both SOL1 and SOL2. The average NTVOCs/OM_{sv} ratios for high and low temperature experiments are reported together with the standard deviation in Table 3. For SOL1 we calculated an average ratio of 4.2±1.1 at high temperatures and 7.2±2.6 for low temperatures. SOL2 reduces the differences in the average NTVOCs/OM_{sv} ratios at the two temperatures, and therefore will be used to describe the dependency of the primary organic compounds. For SOL2 the overall NTVOCs/OM_{sv} ratio between high and low temperature experiments is around 4.75. Figure 4 shows the resolved equilibrium phase partitioning (Eq. 1) between the gas and particle phase at the beginning of each of the 11 smog chamber experiments ($OA_{t=0}$) using SOL2. As expected, most of the material is found in the gas-phase at high temperatures, while at lower temperature only part of the compounds with saturation concentrations (at 20°C) between 100 and 1000 μg m^{-3} would reside in the gas-phase.

3.1.2 Modelling of wood burning aging at low and high temperature

In this section we will focus on the emission aging. Using the NTVOCs/OM_{sv} ratio and the enthalpies of vaporization retrieved in section 3.1.1, we modelled the eight different smog chamber experiments: No. 1, 2, 3, 4 (low temperature) and No. 8, 9, 10, 11 (high temperature) performed at the same relative humidity (RH = 50%). For each of the eight experiments we injected an average mixture of NTVOCs equal to 4.75 times the OM_{sv} mass before the start of the aging. NTVOCs react solely with OH, whose concentration was retrieved from PTR-MS measurements. The temperature dependence of the reaction rates was also taken into account through the Arrhenius equation. The reaction rates ($k_{OH\text{-}NTVOCs}$) and yields (Y) of the NTVOCs as well as enthalpies of vaporization of SOA (ΔH_{vapSOA}) for set2 and set3 were varied within specific physically realistic ranges. We varied $k_{OH\text{-}NTVOCs}$ between 2 and 4 x 10^{-11} cm^3 $molec^{-1}$ s^{-1} in steps of 0.1 x 10^{-11} cm^3 $molec^{-1}$ s^{-1}, and yields between 0.1 and 0.4 ppm ppm^{-1} in steps of 0.01 ppm ppm^{-1}. Values for ΔH_{vapSOA} are still highly uncertain. In this study we explored a wide range of values from 15,000 J mol^{-1} to 115,000 J mol^{-1} in steps of 20,000 J mol^{-1}. The model performance for each combination of i,j and k was evaluated in terms of the root mean square error (RMSE) for the eight experiments and a best fitting solution retrieved as the one that minimized the sum of the errors on both the O:C ratio and OA mass (giving the same weight on both quantities). We performed a total number of $(i \times j \times k \times n_{exp}) = (21 \times 31 \times 6 \times 8) = 31248$ simulations, where n_{exp} are the numbers of aging experiments. Figure 5 shows the total errors for the OA mass (left side) and O:C ratio (right

Geosci. Model Dev. Discuss., doi:10.5194/gmd-2016-163, 2016
Manuscript under review for journal Geosci. Model Dev.
Published: 11 August 2016
© Author(s) 2016. CC-BY 3.0 License.

side) for different ΔH_{vapSOA}, Y and $k_{OH\text{-}NTVOCs.}$ These global errors are root mean squared deviations (i.e. for the eight experiments) adjusted to the number of points per experiment. The error on the OA mass varies from a minimum of ~25% up to more than 60 % whereas the errors on the O:C ratio (Figure 5 right side) are lower and they range from approximately 15 % up to more than 30 %. For the OA mass, distinct regions with lower errors are visible in the central part of each panel with different ΔH_{vapSOA}, representing the models that fitted best the measured OA. While a similar observation can be made for the O:C, models with high ΔH_{vapSOA} tend to reproduce the data less faithfully. The diamonds in Figure 5 indicate the absolute best fitting solution (in yellow) and the ones retrieved with a likelihood-ratio test allowing for 10% error form the best fit (red diamonds). Regions with lower error are localized for $k_{OH\text{-}NTVOCs} \geq 2.5 \times 10^{-11}$ cm^3 molec^{-1} s^{-1} between ΔH_{vapSOA} values of 35,000 and 55,000 J mol^{-1}.

Figure 6 shows the modelled and measured OA mass for all the 8 aging experiments. The primary organic aerosol fraction is reported as well as the SOA fraction from SVOCs and higher volatility NTVOCs. All the low temperature experiments (No. 1, 2, 3, 4 left side of the panel) were reproduced very well along with the concentration gradients at the end of each the experiments even though the model tends in general to slightly over-predict the final OA concentration. The primary fraction slightly increases at the very beginning of the aging phase and it decreases as the experiments proceed as a result of its partitioning to the gas phase and subsequent oxidation. Most of the SOA was predicted to be formed from NTVOCs precursors and only a minor amount from SVOCs. On the other hand, for experiments conducted at higher temperature (No. 8, 9, 10, 11) the OA mass was under-predicted except for experiment No. 8 (see also Figure S1). In this case, SVOCs contribute more significantly to SOA formation compared to low temperature experiments, although the majority of SOA still arises from NTVOCs.

Comparisons between measured and modelled O:C ratios are reported in Fig. 7. Model and observation results match very well, especially upon aging. Significant differences between measured and modelled O:C ratios at the beginning of the experiments highlight on the one hand the variable nature of primary biomass smoke emissions. This variability cannot be accounted for in the model. On the other hand, for some experiments the model under-predicts the measured O:C ratios suggesting that the model parameters describing the O:C of primary emissions are suboptimal. These parameters include directly the carbon and oxygen

Geosci. Model Dev. Discuss., doi:10.5194/gmd-2016-163, 2016
Manuscript under review for journal Geosci. Model Dev.
Published: 11 August 2016
© Author(s) 2016. CC-BY 3.0 License.

number of species in set 1, and indirectly the volatility distributions and enthalpy of vaporization, which are all adopted from previous published data. The average bias in POA O:C ratios is ~30%, well within the experimental uncertainties.

4 Implications for large-scale models

We performed extensive box model simulations of wood burning experiments conducted at two different temperatures (263 and 288 K) in a ~7 m^3 smog chamber facility. By combining new NTVOCs measurements and already available partitioning data for primary wood burning emission, we constrained the amounts of NTVOCs that act as SOA precursors. Our estimates indicate that NTVOCs are approximately 4.75 times the amount of total organic material in the 0.1 and 1000 µg m^{-3} saturation concentration range (OM_{sv}). This ratio can be directly used in CTM models in the absence of explicit NTVOCs emissions for wood burning in combination with the proposed aging scheme. Specific parameters such as NTVOCs reaction rates ($k_{OH\text{-}NTVOCs}$), yields (Y) and enthalpies of vaporization of secondary organic aerosol (ΔH_{vapSOA}) were varied using brute force simulations, and their values were retrieved for best fitting solutions falling within a physically realistic range. The model predicted that the majority of the SOA formed during the aging-phase arose from NTVOCs precursors and only a smaller amount from SVOCs.

Based on our best fitting solutions, we can now predict the OA mass and composition as well as SOA yields at any given temperature, emission load and OH exposure. This is illustrated in Figure 8 for 3 different OM emission loads (OM_{sv} + NTVOCs) of 6, 60 and 600 µg m^{-3} and for a wide range of atmospherically relevant temperatures (from 253.15 K to 313.15 K).

Partitioning of POA depends on the temperature and the injection amounts. The primary organic aerosol mass (POA) decreases with temperature by ~0.5% K^{-1} on average with higher effects predicted at higher loads (0.7% K^{-1} at 600 µg m^{-3}, 0.3% at 6 µg m^{-3}). The partitioning coefficient of the primary material increases by about a factor of 1.5 for a 10-fold increase in the emissions. As aging proceeds, POA mass slightly increases as a result of additional partitioning, but after an OH exposure of (1.0-1.5) x 10^7 molec cm^{-3} h, the trend is inversed and POA mass decreases due to the oxidation of semi-volatile primary compounds. This effect is more visible at high loads.

From Figure 8, we can also assess the impact of temperature, OH exposure and emission concentrations on SOA yields. The temperature effect on SOA yields is a function of OH

Geosci. Model Dev. Discuss., doi:10.5194/gmd-2016-163, 2016
Manuscript under review for journal Geosci. Model Dev.
Published: 11 August 2016
© Author(s) 2016. CC-BY 3.0 License.

exposure, aerosol load, and temperature: i.e. $\partial Y/\partial T = f(T, C_{OA}, OH_{exp})$. SOA yields increase by 0.03, 0.06 and 0.05 % K^{-1} on average for 6, 60 and 600 μg m^{-3} respectively, with higher effects predicted in general at lower temperatures. The temperature effect on the yields is also greater at higher OH exposures (except for very high loads). An analysis typically performed to estimate the volatility distribution of SOA products is based on SOA yields from chamber data performed at different precursor concentrations. We investigated the impact of the OA concentration on the yield at different temperatures and OH exposure. In Figure S2, an average change in the yield with $\log C_{OA}$ is shown at the different conditions: $(\partial Y/\partial \log C_{OA}) = f(T, OH_{exp})$. Note that an increase in SOA yields with the $\log C_{OA}$ was observed as expected. This increase is not solely due to additional partitioning, but is partially also related to changes in the actual chemical composition and hence volatility distribution of the SOA surrogates, as they age to different extents at different concentrations and different temperatures. We determined a yield increase of 4-9% for a 10-fold increase in emissions, with a higher effect at higher OH exposures and lower temperatures.

From Figure 8, one may evaluate the minimum OH exposure values required for SOA to exceed POA. SOA is predicted to exceed POA after~1.5 x 10^7 molec cm^{-3} h, for typical ambient concentrations and temperatures. At low temperatures (263 K) and high loads, SOA might exceed POA at an OH exposure of 9 x 10^6 molec cm^{-3} h, or in 2-10 hours (at OH concentrations of (1-5) x 10^6 molec cm^{-3}), in line with our previously estimated values for biomass burning emissions for the typical conditions of haze events (Huang et al., 2014). Comparatively, at 288.15K an OH exposure of 7 x 10^6 molec cm^{-3} h would be required for SOA to exceed POA, which might be reached within 2 hours or less at typical summer OH concentrations, i.e. (5-10) x 10^6 molec cm^{-3}. These results confirm previous observations that SOA formation is very rapid and the SOA fraction might exceed primary emissions within time-scales of hours, even during haze events.

Geosci. Model Dev. Discuss., doi:10.5194/gmd-2016-163, 2016
Manuscript under review for journal Geosci. Model Dev.
Published: 11 August 2016
© Author(s) 2016. CC-BY 3.0 License.

Acknowledgements

This study was financially supported by the Swiss Federal Office of Environment (FOEN). I. El Haddad was financially supported by the Swiss National Science Foundation. We appreciate the availability of VBS framework in CAMx and support of RAMBOLL ENVIRON.

Code and/or data availability

The VBS box model was written in fortran and was compiled using the Portland group compilers. Simulations were performed under Scientific Linux SL distribution using C shell scripts in order to brute force the chemical and physical parameters. Model output was written in tab-separated text format. Routines to perform the oxidation reactions of SOA precursors and partitioning between particle and gas-phase phase organic material were taken from the CAMx model (available at http://www.camx.com/) and based on the work of Koo et al. (2014). Please contact the corresponding author of this publication if you are interested in model application and/or scientific collaboration.

Geosci. Model Dev. Discuss., doi:10.5194/gmd-2016-163, 2016
Manuscript under review for journal Geosci. Model Dev.
Published: 11 August 2016
© Author(s) 2016. CC-BY 3.0 License.

Tables and Figures

Table 1. Properties of the VBS space. Oxygen numbers for each volatility bin were calculated using the group-contribution of Donahue et al. (2011). Hydrogen numbers were calculated from the van Krevelen relation (Heald et al., 2010).

	Log (C*)	Oxygen number	Carbon number	Hydrogen number	O:C ratio	Molecular weight
POA set1	-1	4.11	11.00	17.89	0.37	216
	0	3.43	11.75	20.07	0.29	216
	1	2.73	12.50	22.27	0.22	216
	2	2.01	13.25	24.49	0.15	216
	3	1.27	14.00	26.73	0.09	215
SOA set2	-1	4.53	9.00	13.47	0.50	194
	0	4.00	9.25	14.50	0.43	189
	1	3.40	9.50	15.60	0.36	184
	2	2.83	9.75	16.67	0.29	179
	3	2.26	10.00	17.74	0.23	174
SOA set3	-1	5.25	5.00	4.75	1.05	149
	0	4.70	5.25	5.80	0.90	144
	1	4.20	5.50	6.80	0.76	140
	2	3.65	5.75	7.85	0.63	135
	3	3.15	6.00	8.85	0.52	131

Geosci. Model Dev. Discuss., doi:10.5194/gmd-2016-163, 2016
Manuscript under review for journal Geosci. Model Dev.
Published: 11 August 2016
© Author(s) 2016. CC-BY 3.0 License.

Geoscientific Model Development Discussions
Open Access
EGU

Table 2. Modelled and experimental data for 11 wood burning experiments. OM_{sv} mass at the beginning of each chamber experiments are reported together with measured $OA_{t=0}$ and the initial NTVOCs concentration. The (NTVOCs)/(OM_{sv}) indicates the ratio between the measured NTVOCs and the imposed OM_{sv} mass at the beginning of each experiment for the two different ΔH_{vapPOA} solutions (SOL1 and SOL2).

	Exp1 T=263 K RH=50%	Exp2 T=263 K RH=50%	Exp3 T=263 K RH=50%	Exp4 T=263 K RH=50%	Exp5 T=263 K RH=90%	Exp6 T=263 K RH=90%	Exp7 T=263 K RH=90%	Exp8 T=288 K RH=50%	Exp9 T=288 K RH=50%	Exp10 T=288 K RH=50%	Exp11 T=288 K RH=50%
Measured IVOC [$\mu g/m^3$]	185.1	-	-	79.3	143.5	91.7	68.7	121.5	190.4	174.6	195.7
Measured $OA_{t=0}$ [$\mu g/m^3$]	12.3	8.1	16.7	9.3	12.0	17.7	6.0	22.6	17.5	18.7	18.6
SOL1 Modelled OM_{sv} [$\mu g/m^3$]	17.3	12.1	22.4	13.6	16.9	23.5	9.5	46.6	37.7	39.8	39.6
SOL2 Modelled OM_{sv} [$\mu g/m^3$]	22.7	15.8	29.5	17.8	22.2	31.0	12.3	49.7	40.1	42.4	42.2
SOL1 (NTVOCs)/(OM_{sv})	10.7	-	-	5.1	8.5	3.9	7.2	2.6	5.0	4.4	4.9
SOL2 (NTVOCs)/(OM_{sv})	8.1	-	-	4.4	6.4	3.0	5.6	2.4	4.7	4.1	4.6

Geosci. Model Dev. Discuss., doi:10.5194/gmd-2016-163, 2016
Manuscript under review for journal Geosci. Model Dev.
Published: 11 August 2016
© Author(s) 2016. CC-BY 3.0 License.

Geoscientific Model Development Discussions
Open Access
EGU

435 Table 3. Solutions used for primary organic aerosol enthalpies of vaporization with averages
436 and standard deviations of the $(NTVOCs)/(OM_{sv})$ ratio..

437

ΔH_{vapPOA} (kJ mol^{-1})	(NTVOCs)/(OM_{sv}) Average High-T (288 K)	(NTVOCs)/(OM_{sv}) Average Low-T (263 K)
SOL1 $-4\log_{10}(C^{*}_{298K}) + 85$	4.2±1.1	7.2±2.6
SOL2 $-11\log_{10}(C^{*}_{298K}) + 70$	4.0±1.1	5.5±2.0

438

439

Geosci. Model Dev. Discuss., doi:10.5194/gmd-2016-163, 2016
Manuscript under review for journal Geosci. Model Dev.
Published: 11 August 2016
© Author(s) 2016. CC-BY 3.0 License.

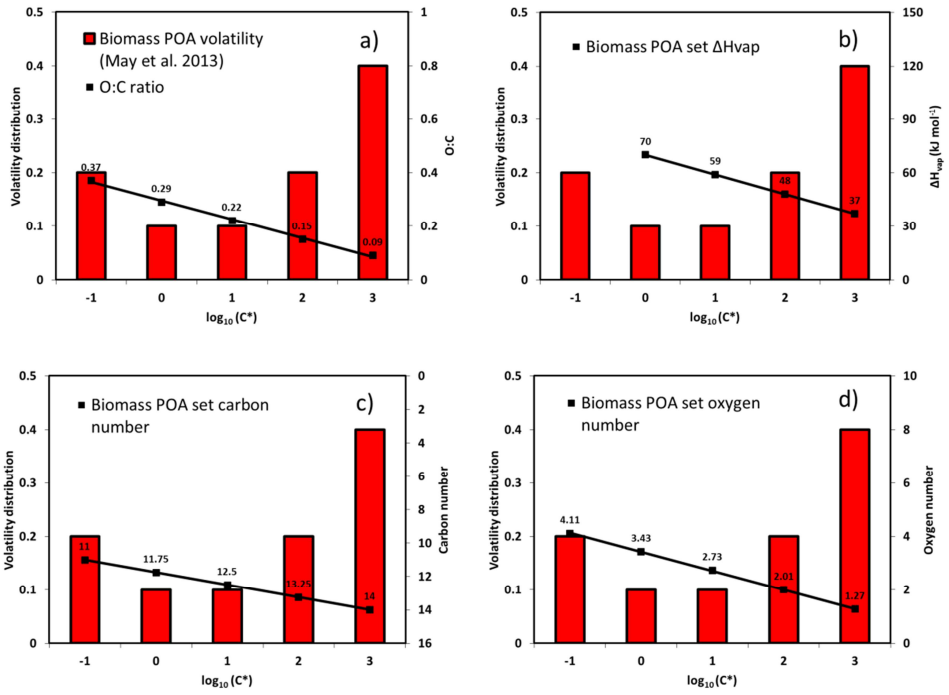

Figure 1. Properties of the wood burning POA set. a) O:C ratio, b) ΔH_{vap} c) C number d) O number. Volatility distribution and enthalpies of vaporization were taken from May et al. (2013). Carbon and oxygen numbers were calculated using the group contribution approach of Donahue et al. (2011). Wood burning POA carbon numbers were placed from 14 to 11 and linearly interpolated between the volatility bins.

Geosci. Model Dev. Discuss., doi:10.5194/gmd-2016-163, 2016
Manuscript under review for journal Geosci. Model Dev.
Published: 11 August 2016
© Author(s) 2016. CC-BY 3.0 License.

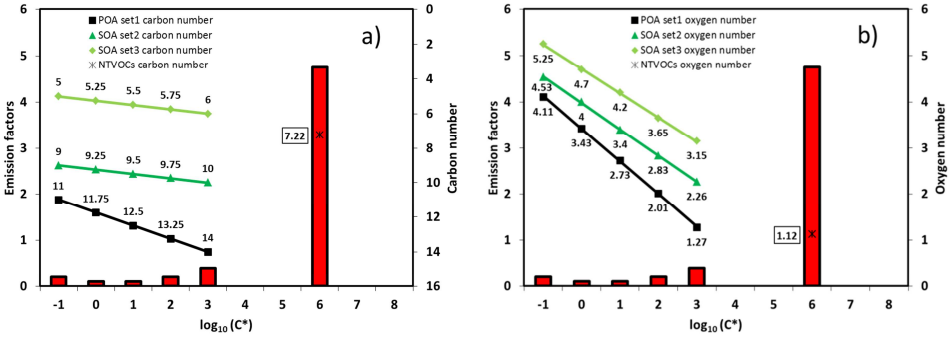

Figure 2. Properties of the wood burning POA and SOA sets. a) C number b) O number. Wood burning SOA carbon numbers were placed from 10 to 5 and linearly interpolated between the volatility bins. Oxygen numbers were calculated using the group approach of Donahue et al. (2011). NTVOCs carbon and oxygen numbers were retrieved from PTR-MS data The red bars indicate the OM emission factors.

Geosci. Model Dev. Discuss., doi:10.5194/gmd-2016-163, 2016
Manuscript under review for journal Geosci. Model Dev.
Published: 11 August 2016
© Author(s) 2016. CC-BY 3.0 License.

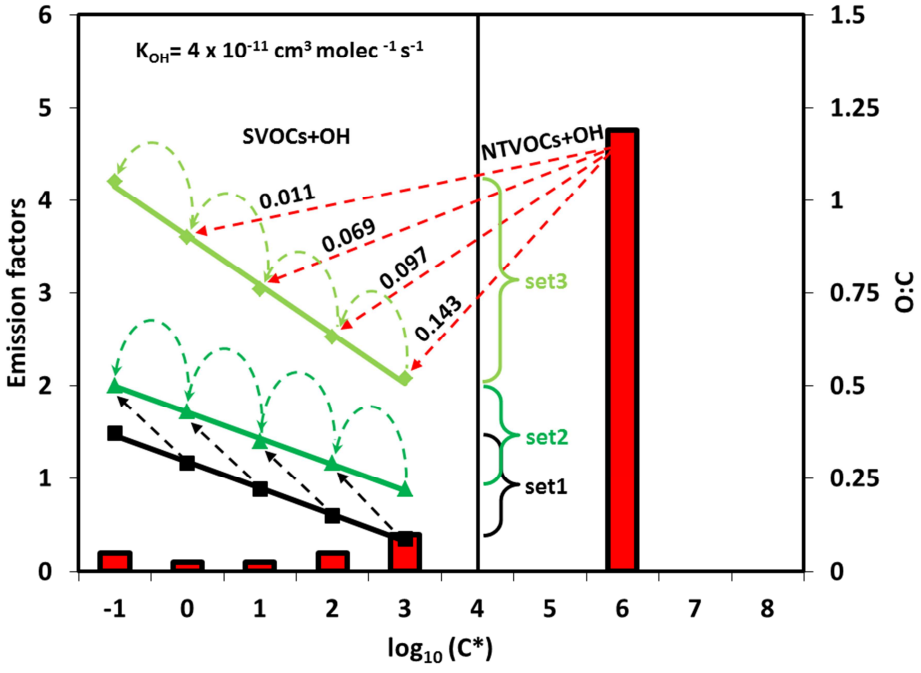

455

456 Figure 3. Proposed oxidation scheme: an average mixture of NTVOCs compounds are
457 allowed to react with the hydroxyl radical following a naphthalene kernel mass distribution.
458 Secondary products in the SOA set (set3) are allowed to further react with a reaction rate of
459 k_{OH} = 4.0 x 10^{-11} cm^3 $molec^{-1}$ s^{-1}. Oxidation products from semi-volatile vapours from the
460 POA set (set1) are allowed for further aging in set2. The numbers on the red arrows indicate
461 the NTVOCs yields for each bin for the best fitting solution (ppm ppm^{-1}).

462

Geosci. Model Dev. Discuss., doi:10.5194/gmd-2016-163, 2016
Manuscript under review for journal Geosci. Model Dev.
Published: 11 August 2016
© Author(s) 2016. CC-BY 3.0 License.

Geoscientific Model Development Discussions
Open Access
EGU

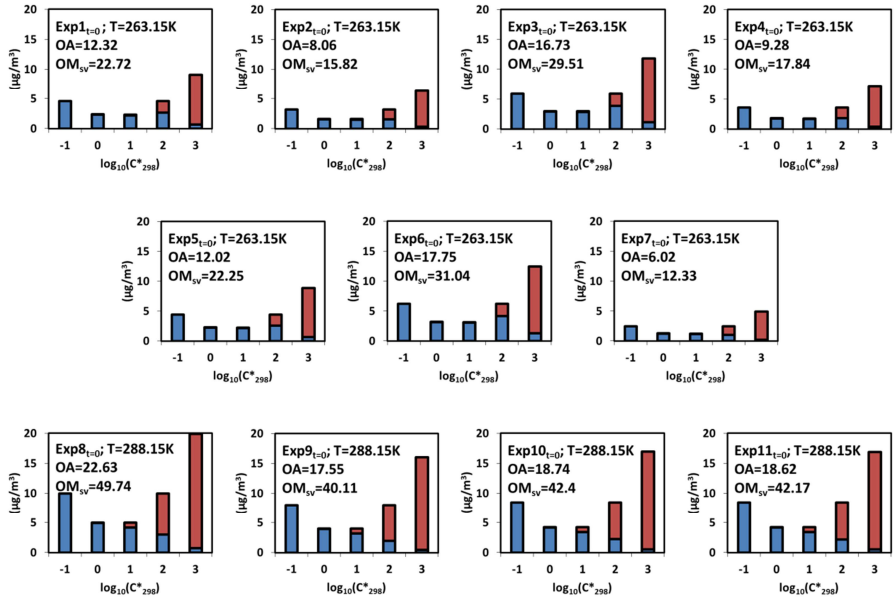

Figure 4. Partitioning of wood burning POA before the start of the aging for 11 smog chamber experiments (SOL2). Gas-phase in red and particle phase in blue.

Geosci. Model Dev. Discuss., doi:10.5194/gmd-2016-163, 2016
Manuscript under review for journal Geosci. Model Dev.
Published: 11 August 2016
© Author(s) 2016. CC-BY 3.0 License.

Geoscientific Model Development Discussions

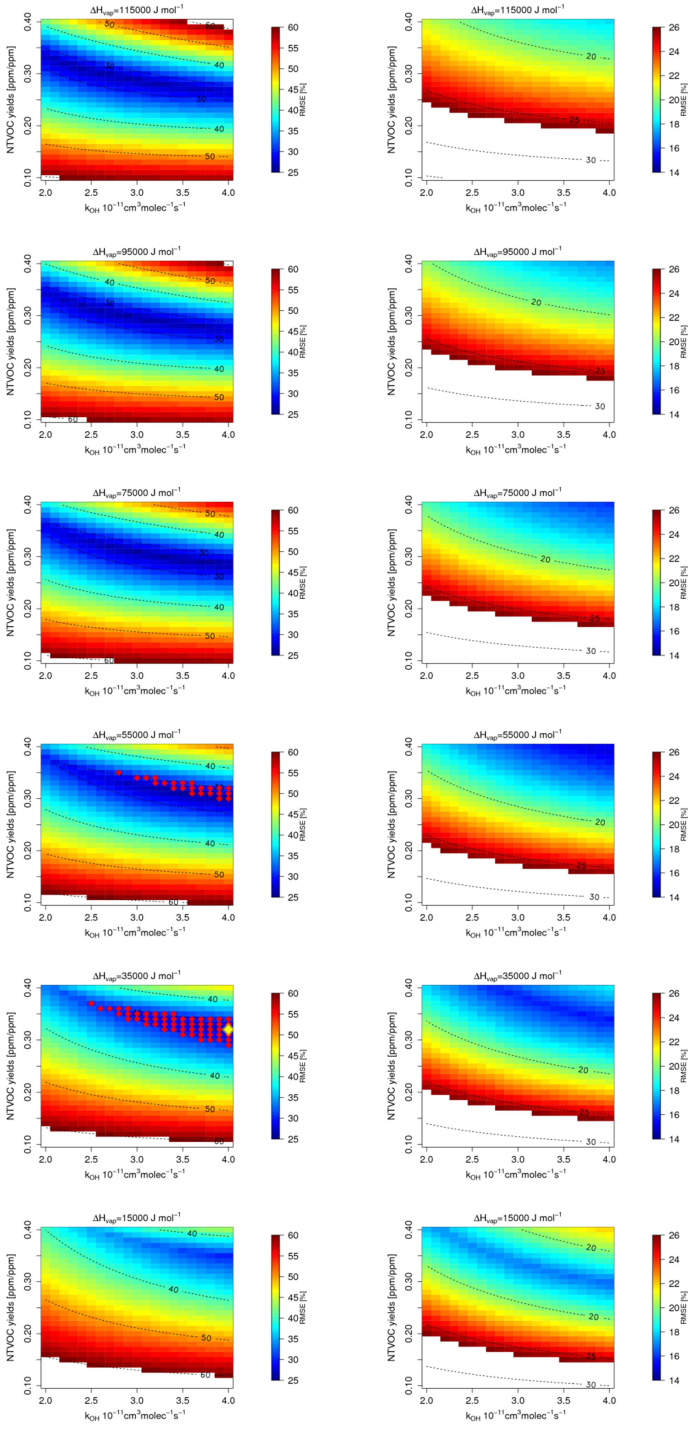

Geosci. Model Dev. Discuss., doi:10.5194/gmd-2016-163, 2016
Manuscript under review for journal Geosci. Model Dev.
Published: 11 August 2016
© Author(s) 2016. CC-BY 3.0 License.

476 Figure 5. Total error on the OA mass (left side) and on the O:C ratio (right side). White
477 regions have an error larger than 60% for the OA mass and 26% for the O:C ratio. The
478 number of simulations per experiment is 3906. The red diamonds indicate the likelihood ratio
479 test results for solutions within 10% error from the best one (yellow diamond).

Geosci. Model Dev. Discuss., doi:10.5194/gmd-2016-163, 2016
Manuscript under review for journal Geosci. Model Dev.
Published: 11 August 2016
© Author(s) 2016. CC-BY 3.0 License.

480

481

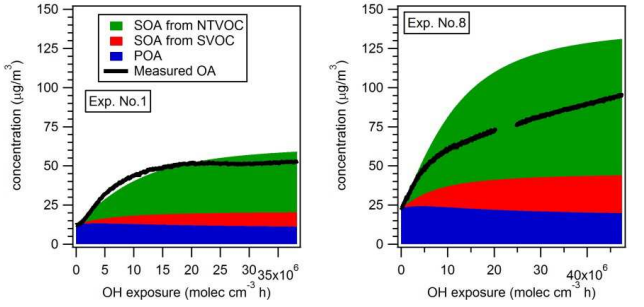

482

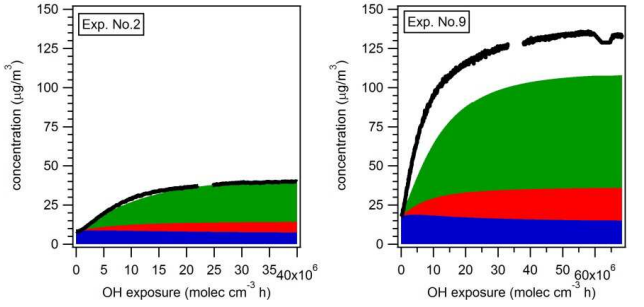

483

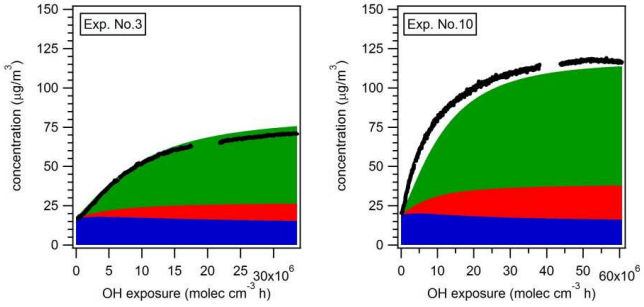

484

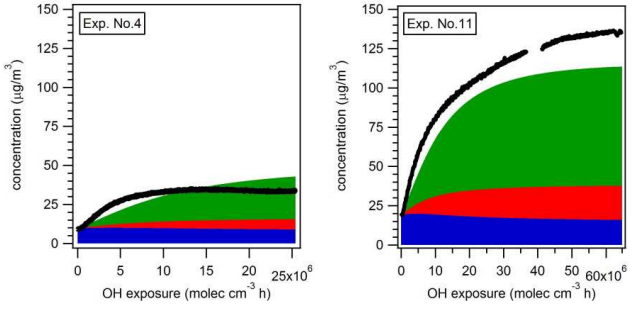

485 Figure 6. Modelled and observed OA mass for low temperature experiments (left side) and
486 high temperature experiments (right side). The model results for the best fitting solution

Geosci. Model Dev. Discuss., doi:10.5194/gmd-2016-163, 2016
Manuscript under review for journal Geosci. Model Dev.
Published: 11 August 2016
© Author(s) 2016. CC-BY 3.0 License.

Geoscientific Model Development Discussions

(yellow diamond in Figure 5). SOA from NTVOCs and SVOCs as well as POA are reported in green, red and blue, respectively.

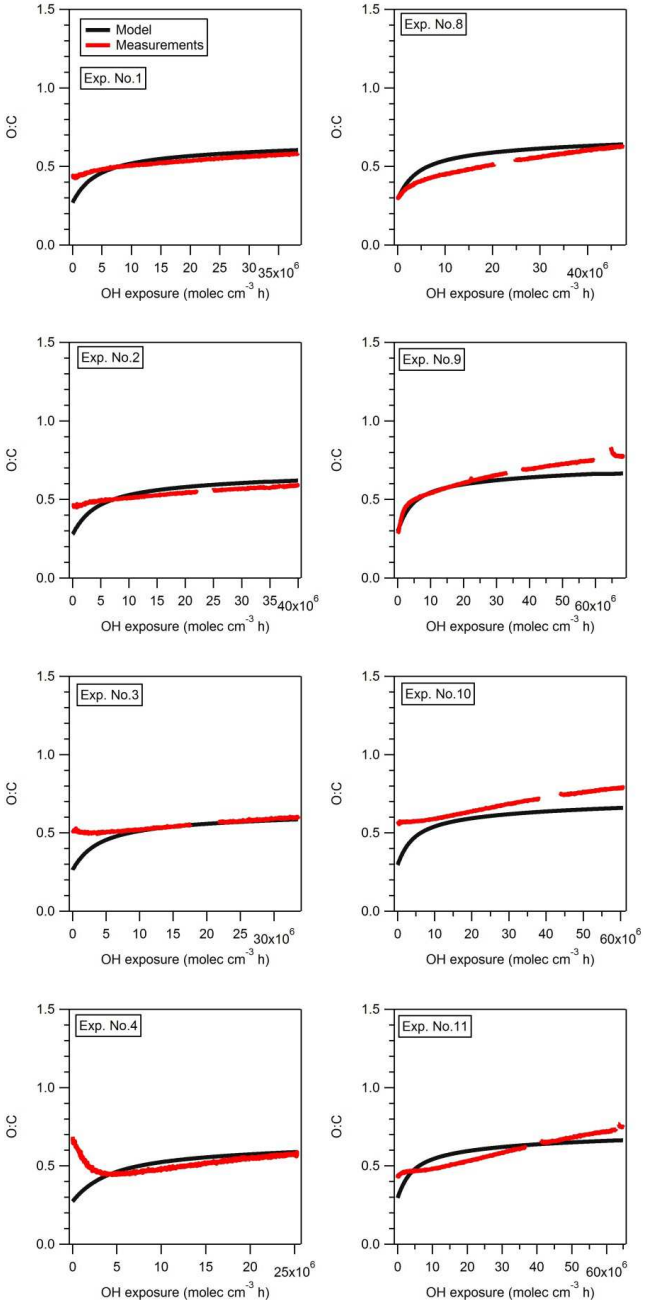

Geosci. Model Dev. Discuss., doi:10.5194/gmd-2016-163, 2016
Manuscript under review for journal Geosci. Model Dev.
Published: 11 August 2016
© Author(s) 2016. CC-BY 3.0 License.

Geoscientific Model Development Discussions

494 Figure 7. Modelled (black lines) and observed (red lines) O:C ratio for low temperature
495 experiments (left side) and high temperature experiments (right side).
496

497 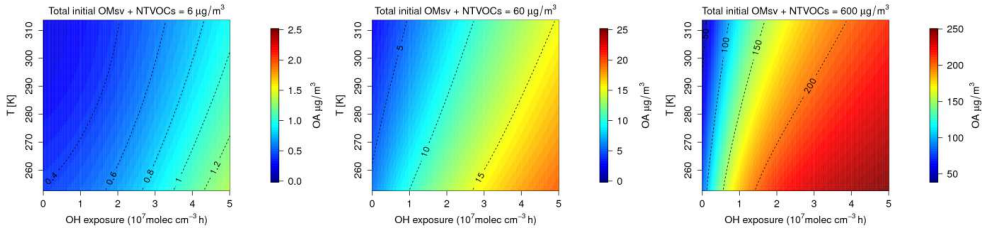

498 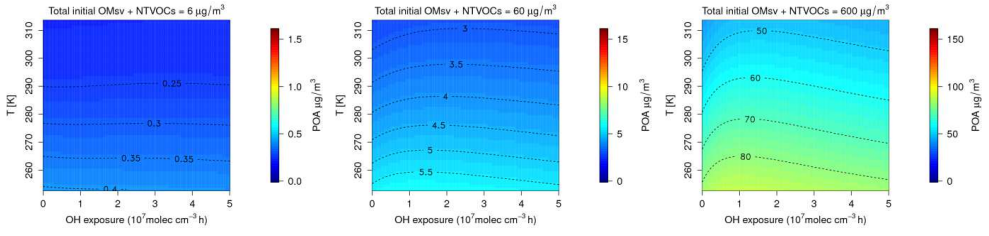

499 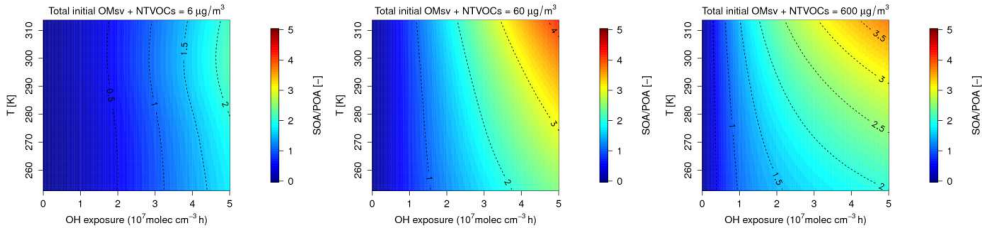

500 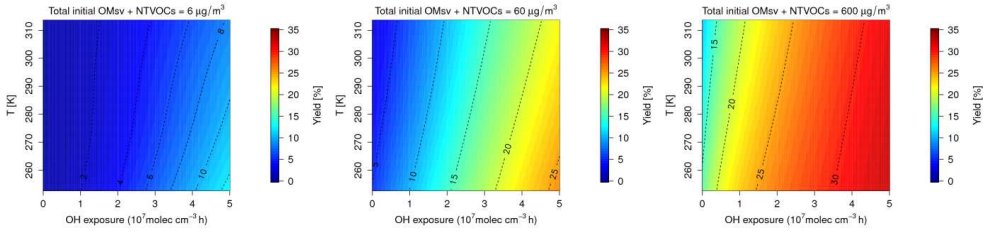

501 Figure 8. Predicted OA mass (upper panels, note different scales), POA mass, SOA/POA ratio
502 (middle panels) and yields (lower panels) at different OMsv + NTVOCs initial load and
503 atmospheric conditions (*T*).
504

Geosci. Model Dev. Discuss., doi:10.5194/gmd-2016-163, 2016
Manuscript under review for journal Geosci. Model Dev.
Published: 11 August 2016
© Author(s) 2016. CC-BY 3.0 License.

505 **References**

506 Barmet, P., Dommen, J., DeCarlo, P. F., Tritscher, T., Praplan, A. P., Platt, S. M., Prévôt, A.
507 S. H., Donahue, N. M. and Baltensperger, U.: OH clock determination by proton transfer
508 reaction mass spectrometry at an environmental chamber, Atmos. Meas. Tech., 5(3), 647–
509 656, doi:10.5194/amt-5-647-2012, 2012.

510 Bergström, R., Denier van der Gon, H. A. C., Prévôt, A. S. H., Yttri, K. E. and Simpson, D.:
511 Modelling of organic aerosols over Europe (2002–2007) using a volatility basis set (VBS)
512 framework: application of different assumptions regarding the formation of secondary organic
513 aerosol, Atmos. Chem. Phys., 12(18), 8499–8527, doi:10.5194/acp-12-8499-2012, 2012.

514 Bessagnet, B., Colette, A., Meleux, F., Rouïl, L., Ung, A., Favez, O., Cuvelier, C., Thunis, P.,
515 Tsyro, S., Stern, R., Manders, A., Kranenburg, R., Aulinger, A., Bieser, J., Mircea, M.,
516 Briganti, A., Cappelletti, A., Calori, G., Finardi, S., Silibello, C., Ciarelli, G., Aksoyoglu, S.,
517 Prévôt, A., Pay, M. T., Baldasano, J. M., García Vivanco, M., Garrido, J. L., Palomino, I.,
518 Martín, F., Pirovano, G., Roberts, P., Gonzalez, L., White, L., Menut, L., Dupont, J. C.,
519 Carnevale, C. and Pederzoli, A.: The EURODELTA III exercise – Model evaluation with
520 observations issued from the 2009 EMEP intensive period and standard measurements in
521 Feb/Mar 2009, 2014.

522 Bruns, E. A., Krapf, M., Orasche, J., Huang, Y., Zimmermann, R., Drinovec, L., Močnik, G.,
523 El-Haddad, I., Slowik, J. G., Dommen, J., Baltensperger, U. and Prévôt, A. S. H.:
524 Characterization of primary and secondary wood combustion products generated under
525 different burner loads, Atmos. Chem. Phys., 15(5), 2825–2841, doi:10.5194/acp-15-2825-
526 2015, 2015.

527 Bruns, E. A., El Haddad, I., Slowik, J. G., Kilic, D., Klein, F., Baltensperger, U. and Prévôt,
528 A. S. H.: Identification of significant precursor gases of secondary organic aerosols from
529 residential wood combustion, Sci. Rep., 6, 27881, doi:10.1038/srep27881, 2016.

530 Canonaco, F., Slowik, J. G., Baltensperger, U. and Prévôt, A. S. H.: Seasonal differences in
531 oxygenated organic aerosol composition: implications for emissions sources and factor
532 analysis, Atmos. Chem. Phys., 15(12), 6993–7002, doi:10.5194/acp-15-6993-2015, 2015.

533 Ciarelli, G., Aksoyoglu, S., Crippa, M., Jimenez, J. L., Nemitz, E., Sellegri, K., Äijälä, M.,
534 Carbone, S., Mohr, C., O'Dowd, C., Poulain, L., Baltensperger, U. and Prévôt, A. S. H.:
535 Evaluation of European air quality modelled by CAMx including the volatility basis set
536 scheme, Atmos. Chem. Phys., in press, 2016.

537 Crippa, M., DeCarlo, P. F., Slowik, J. G., Mohr, C., Heringa, M. F., Chirico, R., Poulain, L.,
538 Freutel, F., Sciare, J., Cozic, J., Di Marco, C. F., Elsasser, M., Nicolas, J. B., Marchand, N.,
539 Abidi, E., Wiedensohler, A., Drewnick, F., Schneider, J., Borrmann, S., Nemitz, E.,
540 Zimmermann, R., Jaffrezo, J.-L., Prévôt, A. S. H. and Baltensperger, U.: Wintertime aerosol
541 chemical composition and source apportionment of the organic fraction in the metropolitan
542 area of Paris, Atmos. Chem. Phys., 13(2), 961–981, doi:10.5194/acp-13-961-2013, 2013.

543 Denier van der Gon, H. A. C., Bergström, R., Fountoukis, C., Johansson, C., Pandis, S. N.,
544 Simpson, D. and Visschedijk, A. J. H.: Particulate emissions from residential wood

© Author(s) 2016. CC-BY 3.0 License.

545 combustion in Europe – revised estimates and an evaluation, Atmos. Chem. Phys., 15(11),
546 6503–6519, doi:10.5194/acp-15-6503-2015, 2015.

547 Donahue, N. M., Robinson, A. L., Stanier, C. O. and Pandis, S. N.: Coupled Partitioning,
548 Dilution, and Chemical Aging of Semivolatile Organics, Environ. Sci. Technol., 40(8), 2635–
549 2643, doi:10.1021/es052297c, 2006.

550 Donahue, N. M., Epstein, S. A., Pandis, S. N. and Robinson, A. L.: A two-dimensional
551 volatility basis set: 1. organic-aerosol mixing thermodynamics, Atmos. Chem. Phys., 11(7),
552 3303–3318, doi:10.5194/acp-11-3303-2011, 2011.

553 Donahue, N. M., Kroll, J. H., Pandis, S. N. and Robinson, A. L.: A two-dimensional volatility
554 basis set – Part 2: Diagnostics of organic-aerosol evolution, Atmos. Chem. Phys., 12(2), 615–
555 634, doi:10.5194/acp-12-615-2012, 2012.

556 Donahue, N. M., Chuang, W., Epstein, S. A., Kroll, J. H., Worsnop, D. R., Robinson, A. L.,
557 Adams, P. J. and Pandis, S. N.: Why do organic aerosols exist? Understanding aerosol
558 lifetimes using the two-dimensional volatility basis set, Environ. Chem., 10(3), 151,
559 doi:10.1071/EN13022, 2013.

560 Drinovec, L., Močnik, G., Zotter, P., Prévôt, A. S. H., Ruckstuhl, C., Coz, E., Rupakheti, M.,
561 Sciare, J., Müller, T., Wiedensohler, A. and Hansen, A. D. A.: The "dual-spot" Aethalometer:
562 an improved measurement of aerosol black carbon with real-time loading compensation,
563 Atmos. Meas. Tech., 8(5), 1965–1979, doi:10.5194/amt-8-1965-2015, 2015.

564 Fountoukis, C., Megaritis, A. G., Skyllakou, K., Charalampidis, P. E., Pilinis, C., Denier van
565 der Gon, H. A. C., Crippa, M., Canonaco, F., Mohr, C., Prévôt, A. S. H., Allan, J. D., Poulain,
566 L., Petäjä, T., Tiitta, P., Carbone, S., Kiendler-Scharr, A., Nemitz, E., O'Dowd, C., Swietlicki,
567 E. and Pandis, S. N.: Organic aerosol concentration and composition over Europe: insights
568 from comparison of regional model predictions with aerosol mass spectrometer factor
569 analysis, Atmos. Chem. Phys., 14(17), 9061–9076, doi:10.5194/acp-14-9061-2014, 2014.

570 Grieshop, A. P., Logue, J. M., Donahue, N. M. and Robinson, A. L.: Laboratory investigation
571 of photochemical oxidation of organic aerosol from wood fires 1: measurement and
572 simulation of organic aerosol evolution, Atmos. Chem. Phys., 9(4), 1263–1277,
573 doi:10.5194/acp-9-1263-2009, 2009.

574 Heald, C. L., Kroll, J. H., Jimenez, J. L., Docherty, K. S., DeCarlo, P. F., Aiken, A. C., Chen,
575 Q., Martin, S. T., Farmer, D. K. and Artaxo, P.: A simplified description of the evolution of
576 organic aerosol composition in the atmosphere, Geophys. Res. Lett., 37(8), n/a-n/a,
577 doi:10.1029/2010GL042737, 2010.

578 Heringa, M. F., DeCarlo, P. F., Chirico, R., Tritscher, T., Clairotte, M., Mohr, C., Crippa, M.,
579 Slowik, J. G., Pfaffenberger, L., Dommen, J., Weingartner, E., Prévôt, A. S. H. and
580 Baltensperger, U.: A new method to discriminate secondary organic aerosols from different
581 sources using high-resolution aerosol mass spectra, Atmos. Chem. Phys., 12(4), 2189–2203,
582 doi:10.5194/acp-12-2189-2012, 2012.

583 Huang, R.-J., Zhang, Y., Bozzetti, C., Ho, K.-F., Cao, J.-J., Han, Y., Daellenbach, K. R.,
584 Slowik, J. G., Platt, S. M., Canonaco, F., Zotter, P., Wolf, R., Pieber, S. M., Bruns, E. A.,
585 Crippa, M., Ciarelli, G., Piazzalunga, A., Schwikowski, M., Abbaszade, G., Schnelle-Kreis,

© Author(s) 2016. CC-BY 3.0 License.

586 J., Zimmermann, R., An, Z., Szidat, S., Baltensperger, U., Haddad, I. E. and Prévôt, A. S. H.:
587 High secondary aerosol contribution to particulate pollution during haze events in China,
588 Nature, 514(7521), 218–222, doi:10.1038/nature13774, 2014.

589 Jo, D. S., Park, R. J., Kim, M. J. and Spracklen, D. V.: Effects of chemical aging on global
590 secondary organic aerosol using the volatility basis set approach, Atmos. Environ., 81, 230–
591 244, doi:10.1016/j.atmosenv.2013.08.055, 2013.

592 Kleindienst, T. E., Lewandowski, M., Offenberg, J. H., Jaoui, M. and Edney, E. O.: Ozone-
593 isoprene reaction: Re-examination of the formation of secondary organic aerosol, Geophys.
594 Res. Lett., 34(1), L01805, doi:10.1029/2006GL027485, 2007.

595 Knote, C., Brunner, D., Vogel, H., Allan, J., Asmi, A., Äijälä, M., Carbone, S., van der Gon,
596 H. D., Jimenez, J. L., Kiendler-Scharr, A., Mohr, C., Poulain, L., Prévôt, A. S. H., Swietlicki,
597 E. and Vogel, B.: Towards an online-coupled chemistry-climate model: evaluation of trace
598 gases and aerosols in COSMO-ART, Geosci. Model Dev., 4(4), 1077–1102,
599 doi:10.5194/gmd-4-1077-2011, 2011.

600 Koo, B., Knipping, E. and Yarwood, G.: 1.5-Dimensional volatility basis set approach for
601 modeling organic aerosol in CAMx and CMAQ, Atmos. Environ., 95, 158–164,
602 doi:10.1016/j.atmosenv.2014.06.031, 2014.

603 Kulmala, M., Asmi, A., Lappalainen, H. K., Carslaw, K. S., Pöschl, U., Baltensperger, U.,
604 Hov, ø., Brenquier, J.-L., Pandis, S. N., Facchini, M. C., Hansson, H.-C., Wiedensohler, A.
605 and O'Dowd, C. D.: Introduction: European Integrated Project on Aerosol Cloud Climate and
606 Air Quality interactions (EUCAARI) – integrating aerosol research from nano to global
607 scales, Atmos. Chem. Phys., 9(8), 2825–2841, doi:10.5194/acp-9-2825-2009, 2009.

608 Kulmala, M., Asmi, A., Lappalainen, H. K., Baltensperger, U., Brenguier, J.-L., Facchini, M.
609 C., Hansson, H.-C., Hov, Ø., O'Dowd, C. D., Pöschl, U., Wiedensohler, A., Boers, R.,
610 Boucher, O., de Leeuw, G., Denier van der Gon, H. A. C., Feichter, J., Krejci, R., Laj, P.,
611 Lihavainen, H., Lohmann, U., McFiggans, G., Mentel, T., Pilinis, C., Riipinen, I., Schulz, M.,
612 Stohl, A., Swietlicki, E., Vignati, E., Alves, C., Amann, M., Ammann, M., Arabas, S., Artaxo,
613 P., Baars, H., Beddows, D. C. S., Bergström, R., Beukes, J. P., Bilde, M., Burkhart, J. F.,
614 Canonaco, F., Clegg, S. L., Coe, H., Crumeyrolle, S., D'Anna, B., Decesari, S., Gilardoni, S.,
615 Fischer, M., Fjaeraa, A. M., Fountoukis, C., George, C., Gomes, L., Halloran, P., Hamburger,
616 T., Harrison, R. M., Herrmann, H., Hoffmann, T., Hoose, C., Hu, M., Hyvärinen, A., Hõrrak,
617 U., Iinuma, Y., Iversen, T., Josipovic, M., Kanakidou, M., Kiendler-Scharr, A., Kirkevåg, A.,
618 Kiss, G., Klimont, Z., Kolmonen, P., Komppula, M., Kristjánsson, J.-E., Laakso, L.,
619 Laaksonen, A., Labonnote, L., Lanz, V. A., Lehtinen, K. E. J., Rizzo, L. V., Makkonen, R.,
620 Manninen, H. E., McMeeking, G., Merikanto, J., Minikin, A., Mirme, S., Morgan, W. T.,
621 Nemitz, E., O'Donnell, D., Panwar, T. S., Pawlowska, H., Petzold, A., Pienaar, J. J., Pio, C.,
622 Plass-Duelmer, C., Prévôt, A. S. H., Pryor, S., Reddington, C. L., Roberts, G., Rosenfeld, D.,
623 Schwarz, J., Seland, Ø., et al.: General overview: European Integrated project on Aerosol
624 Cloud Climate and Air Quality interactions (EUCAARI) – integrating aerosol research from
625 nano to global scales, Atmos. Chem. Phys., 11, 13061–13143, doi:10.5194/acp-11-13061-
626 2011, 2011.

© Author(s) 2016. CC-BY 3.0 License.

Lipsky, E. M. and Robinson, A. L.: Effects of Dilution on Fine Particle Mass and Partitioning of Semivolatile Organics in Diesel Exhaust and Wood Smoke, Environ. Sci. Technol., 40(1), 155–162, doi:10.1021/es050319p, 2006.

May, A. A., Levin, E. J. T., Hennigan, C. J., Riipinen, I., Lee, T., Collett, J. L., Jimenez, J. L., Kreidenweis, S. M. and Robinson, A. L.: Gas-particle partitioning of primary organic aerosol emissions: 3. Biomass burning, J. Geophys. Res. Atmospheres, 118(19), 2013JD020286, doi:10.1002/jgrd.50828, 2013.

Murphy, B. N. and Pandis, S. N.: Simulating the Formation of Semivolatile Primary and Secondary Organic Aerosol in a Regional Chemical Transport Model, Environ. Sci. Technol., 43(13), 4722–4728, doi:10.1021/es803168a, 2009.

Murphy, B. N., Donahue, N. M., Fountoukis, C. and Pandis, S. N.: Simulating the oxygen content of ambient organic aerosol with the 2D volatility basis set, Atmos. Chem. Phys., 11(15), 7859–7873, doi:10.5194/acp-11-7859-2011, 2011.

Nussbaumer, T., Czasch, C., Klippel, N., Johansson, L. and Tullin, C.: Particulate Emissions from Biomass Combustion in IEA Countries, Survey on Measurements and Emission Factors, International Energy Agency (IEA) Bioenergy Task 32, Zurich, 2008a.

Nussbaumer, T., Klippel, N. and Johansson, L.: Survey on Measurements and Emission Factors on Particulate Matter from Biomass Combustion in IEA Countries, 16th European Biomass Conference and Exhibition, Valencia, Spain, 2–6 June 2008, Oral Presentation OA 9.2, 2008b.

Pankow, J. F.: An absorption model of gas/particle partitioning of organic compounds in the atmosphere, Atmos. Environ., 1994.

Pankow, J. F. and Asher, W. E.: SIMPOL.1: a simple group contribution method for predicting vapor pressures and enthalpies of vaporization of multifunctional organic compounds, Atmos. Chem. Phys., 8(10), 2773–2796, doi:10.5194/acp-8-2773-2008, 2008.

Platt, S. M., El Haddad, I., Zardini, A. A., Clairotte, M., Astorga, C., Wolf, R., Slowik, J. G., Temime-Roussel, B., Marchand, N., Ježek, I., Drinovec, L., Močnik, G., Möhler, O., Richter, R., Barmet, P., Bianchi, F., Baltensperger, U. and Prévôt, A. S. H.: Secondary organic aerosol formation from gasoline vehicle emissions in a new mobile environmental reaction chamber, Atmos. Chem. Phys., 13(18), 9141–9158, doi:10.5194/acp-13-9141-2013, 2013.

Robinson, A. L., Donahue, N. M., Shrivastava, M. K., Weitkamp, E. A., Sage, A. M., Grieshop, A. P., Lane, T. E., Pierce, J. R. and Pandis, S. N.: Rethinking Organic Aerosols: Semivolatile Emissions and Photochemical Aging, Science, 315(5816), 1259–1262, doi:10.1126/science.1133061, 2007.

Tørseth, K., Aas, W., Breivik, K., Fjæraa, A. M., Fiebig, M., Hjellbrekke, A. G., Lund Myhre, C., Solberg, S. and Yttri, K. E.: Introduction to the European Monitoring and Evaluation Programme (EMEP) and observed atmospheric composition change during 1972–2009, Atmos. Chem. Phys., 12(12), 5447–5481, doi:10.5194/acp-12-5447-2012, 2012.

© Author(s) 2016. CC-BY 3.0 License.

666 Tsigaridis, K., Daskalakis, N., Kanakidou, M., Adams, P. J., Artaxo, P., Bahadur, R.,
667 Balkanski, Y., Bauer, S. E., Bellouin, N., Benedetti, A., Bergman, T., Berntsen, T. K.,
668 Beukes, J. P., Bian, H., Carslaw, K. S., Chin, M., Curci, G., Diehl, T., Easter, R. C., Ghan, S.
669 J., Gong, S. L., Hodzic, A., Hoyle, C. R., Iversen, T., Jathar, S., Jimenez, J. L., Kaiser, J. W.,
670 Kirkevåg, A., Koch, D., Kokkola, H., Lee, Y. H., Lin, G., Liu, X., Luo, G., Ma, X., Mann, G.
671 W., Mihalopoulos, N., Morcrette, J.-J., Müller, J.-F., Myhre, G., Myriokefalitakis, S., Ng, N.
672 L., O'Donnell, D., Penner, J. E., Pozzoli, L., Pringle, K. J., Russell, L. M., Schulz, M., Sciare,
673 J., Seland, Ø., Shindell, D. T., Sillman, S., Skeie, R. B., Spracklen, D., Stavrakou, T.,
674 Steenrod, S. D., Takemura, T., Tiitta, P., Tilmes, S., Tost, H., van Noije, T., van Zyl, P. G.,
675 von Salzen, K., Yu, F., Wang, Z., Wang, Z., Zaveri, R. A., Zhang, H., Zhang, K., Zhang, Q.
676 and Zhang, X.: The AeroCom evaluation and intercomparison of organic aerosol in global
677 models, Atmos. Chem. Phys., 14(19), 10845–10895, doi:10.5194/acp-14-10845-2014, 2014.

678 Tsimpidi, A. P., Karydis, V. A., Zavala, M., Lei, W., Molina, L., Ulbrich, I. M., Jimenez, J. L.
679 and Pandis, S. N.: Evaluation of the volatility basis-set approach for the simulation of organic
680 aerosol formation in the Mexico City metropolitan area, Atmos. Chem. Phys., 10, 525–546,
681 2010.

682 Waked, A., Favez, O., Alleman, L. Y., Piot, C., Petit, J.-E., Delaunay, T., Verlinden, E.,
683 Golly, B., Besombes, J.-L., Jaffrezo, J.-L. and Leoz-Garziandia, E.: Source apportionment of
684 PM10 in a north-western Europe regional urban background site (Lens, France) using positive
685 matrix factorization and including primary biogenic emissions, Atmos. Chem. Phys., 14(7),
686 3325–3346, doi:10.5194/acp-14-3325-2014, 2014.

687 Zhang, Q. J., Beekmann, M., Drewnick, F., Freutel, F., Schneider, J., Crippa, M., Prevot, A.
688 S. H., Baltensperger, U., Poulain, L., Wiedensohler, A., Sciare, J., Gros, V., Borbon, A.,
689 Colomb, A., Michoud, V., Doussin, J.-F., Denier van der Gon, H. A. C., Haeffelin, M.,
690 Dupont, J.-C., Siour, G., Petetin, H., Bessagnet, B., Pandis, S. N., Hodzic, A., Sanchez, O.,
691 Honoré, C. and Perrussel, O.: Formation of organic aerosol in the Paris region during the
692 MEGAPOLI summer campaign: evaluation of the volatility-basis-set approach within the
693 CHIMERE model, Atmos. Chem. Phys., 13(11), 5767–5790, doi:10.5194/acp-13-5767-2013,
694 2013.

695 Zuend, A. and Seinfeld, J. H.: Modeling the gas-particle partitioning of secondary organic
696 aerosol: the importance of liquid-liquid phase separation, Atmos. Chem. Phys., 12(9), 3857–
697 3882, doi:10.5194/acp-12-3857-2012, 2012.

698